

1 **CO₂ electroreduction to formate: continuous single-pass operation in a**
2 **filter-press reactor at high current densities using Bi Gas Diffusion**
3 **Electrodes**

4
5 G. Díaz-Sainz^{a*}, M. Alvarez-Guerra^a, J. Solla-Gullón^b, L. García-Cruz^b, V. Montiel^b, A. Irabien^a

6
7 ^aUniversidad de Cantabria, Departamento de Ingenierías Química y Biomolecular, ETSIT, Avda. Los Castros s/n,
8 39005, Santander, Spain

9
10 ^bInstituto de Electroquímica, Universidad de Alicante, Apdo. 99, E-03080 Alicante, Spain

11
12 *Corresponding author: diazsg@unican.es

13
14 **Abstract**

15 Electrochemical reduction of CO₂ has been taken into consideration as a fascinating option
16 to store energy from intermittent renewable sources in the form of chemical value-added
17 products. Among the different value-added products, formic acid or formate is
18 particularly attractive since it can be used as a fuel for low-temperature fuel-cells and as
19 a renewable hydrogen carrier. Very recently, a rapidly increasing number of studies have
20 revealed Bi as a promising electrocatalytic material for the CO₂ electroreduction to
21 formate, but the performance of Bi electrodes operating in a continuous mode and high
22 current density (*j*) has been hardly investigated yet. Thus, this work aims at studying the
23 CO₂ electroreduction to formate working in a continuous mode in a filter-press-reactor at
24 a *j* up to 300 mA·cm⁻² using Bi electrodes. Bismuth Gas Diffusion Electrodes (Bi-GDEs)
25 were fabricated from carbon-supported Bismuth-nanoparticles. The influence of *j* and the
26 electrolyte flow/area ratio in the performance of the Bi-GDEs towards formate were

27 evaluated. Working at j of $300 \text{ mA}\cdot\text{cm}^{-2}$, a concentration of $5.2 \text{ g formate}\cdot\text{L}^{-1}$ with a
28 faradaic efficiency (FE) and rate of 70% and $11 \text{ mmol}\cdot\text{m}^{-2}\cdot\text{s}^{-1}$, respectively were
29 achieved. Lowering the j to $90 \text{ mA}\cdot\text{cm}^{-2}$, formate concentrations of up to $7.5 \text{ g}\cdot\text{L}^{-1}$ could
30 be obtained with an excellent FE of 90%. Interestingly, the highest concentration of
31 formate obtained was $18 \text{ g}\cdot\text{L}^{-1}$, but at expenses of an important decrease in FE. Although
32 the results of this study are interesting and promising, further research is required to
33 increase formate concentration for a future implementation at industrial scale.

34 **Keywords**

- 35 - CO_2 electroreduction
- 36 - Bismuth nanoparticles
- 37 - Formate
- 38 - GDEs (Gas diffusion electrodes)
- 39 - Continuous filter-press cell

40

41

42

43

44

45

46

47

48

49 © 2019. This manuscript version is made available under the CC-BY-NC-ND 4.0 license, <http://creativecommons.org/licenses/by-nc-nd/4.0/>

50 **1. Introduction**

51 The concentration of carbon dioxide (CO₂) in the atmosphere has exceeded the limit of 400
52 ppm [1]. It is critical to reduce emissions of CO₂ in order to mitigate climate change [2–
53 4]. CO₂ emissions to atmosphere can be reduced by different strategies, such as improving
54 efficiency in energy use, reducing reliance on carbon-based fuels or strategies based on
55 capture and sequestration of CO₂ (CCS) and capture and utilization of CO₂ (CCU) [5]. In
56 the last years, CO₂ valorisation into products of interest has been considered as an
57 attractive option [6,7], because it allows tackling the problem of reducing CO₂ emissions,
58 and at the same time, the CO₂ conversion into useful products [8,9].

59 CO₂ electroreduction is particularly interesting for CCU, since it is an attractive option
60 for storing the excess of renewable sources of energy (e.g. solar or wind energy) in the
61 form of chemical value-added products [10–15]. One of the main issues for a wider
62 implementation of renewable energy is its intermittence. In this sense, the value-added
63 products obtained by CO₂ electrochemical reduction could be used as fuels, adjusting the
64 production with the consumption and making it possible to store energy for its use when
65 needed (i.e. when there is lack of renewable supply) [16]. Among these value-added
66 products, carbon monoxide (CO) [17,18], hydrocarbons (CH₄ or C₂H₄) [19,20], alcohols
67 (CH₃OH or C₂H₆O) [21,22] or formic acid (HCOOH) [23,24] can be obtained.

68 One of the most engaging products of CO₂ electrocatalytic reduction is formic acid or
69 formate (depending on pH), which is used in a wide variety of industries. Moreover, in
70 the last years, formate is receiving increasing attention due to its use as a renewable
71 hydrogen carrier molecule [25,26] and also as a fuel for fuel-cells [27,28].

72 In previous studies, different materials have been used as electrocatalysts in the
73 electroconversion of CO₂ to give formate, for instance lead [29], indium [30], zinc [17],

74 cobalt [31], palladium [32] and especially tin [33–41]. Very recently, bismuth has started
75 to be considered as a promising electrocatalytic material for the CO₂ electrocatalytic
76 reduction to obtain formate at lower potentials than other metals, with a rapidly growing
77 number studies using Bi in different forms [42-66]. Firstly, Zhang et al. [42] described
78 the use of BiOCl nanosheets under ambient conditions in the electrochemical conversion
79 of CO₂ to give formate with a maximum faradaic efficiency (FE) of 92% and a current
80 density (j) of 3.7 mA·mg⁻¹ at -1.5 V. Additionally, Zhong et al. [43] studied the
81 electrochemical performance for CO₂ towards formate using bismuth dendrites on treated
82 carbon paper as electrocatalyst in the working electrode, achieving a FE of 96.4% with a
83 j of 15.2 mA·cm⁻² at -1.8 V. More recently, the latest studies have performed CO₂
84 electrochemical conversion to formate working with different electrode configurations:
85 electrodes based on bismuth nanoparticles synthesized on copper surface [44,45,65,66];
86 bismuth nanoparticles synthesized on titanium substrate [46] and copper substrate [47];
87 oxide-derived Bi films [48–52,63]; Bi nanosheets [53,54,64] or carbon-supported Bi
88 nanoparticles [55]. All these studies above mentioned have been carried out in an aqueous
89 bicarbonate medium with the exception of Zhang et al. [56] and Atifi et al. [57], which
90 were done in a non-aqueous medium such as MeCN. The studies mentioned previously
91 show promising results, which explains the growing attention to the study of the
92 electrochemical valorisation of CO₂ to obtain formate using Bi as electrocatalyst.
93 However, it is important to note that all these references have studied the CO₂
94 electrocatalytic reduction to give formate in a H-type electrochemical cell with two
95 compartments. In the H-type configuration, both compartments are separated by a piece
96 of membrane (e.g. Nafion 115 [42,43,58], Nafion 117 [44,46,49,53,55,59] or Nafion 212
97 [51,56,57,60,65]), but the catholyte and the anolyte are not pumped to their respective
98 compartments of the electrochemical cell during the CO₂ electroreduction to give

99 formate. High values of FE have been obtained, around 90 % (see Table S1 in the
100 Supporting Information). Although some studies reported formate rate values, neither
101 formate concentration or consumption of energy were provided. As can be seen in Table
102 S1, the maximum j supplied to the electrochemical cell was $60 \text{ mA}\cdot\text{cm}^{-2}$ [58], with the
103 exception of the study by García de Arquer et al. [50]. As a part of a comprehensive work
104 on the characterization of 2D bismuth-based catalyst and the assessment of their
105 performance for CO_2 electroreduction to formate in a three-electrode system and in H-
106 cell setup, Garcia de Arquer et al [50] also mention the use of a flow-cell configuration
107 supplying $200 \text{ mA}\cdot\text{cm}^{-2}$ and giving FE of 90%, but no more details about the flow-cell
108 experiments are reported. As shown in Table S1, previous literature has not worked in a
109 continuous mode with high values of current density supplied. These conditions will be
110 necessary for an application at commercial scale in the future. Moreover, all the literature
111 published using Bi have not reported formate concentration and energy consumption
112 values, essential variables to assess the relevance of the electrochemical process. A study
113 of the influence of variables has not been done either in order to optimise the
114 electrochemical process of CO_2 to formate. In order to develop and improve the use of Bi
115 as catalyst in the CO_2 electroreduction to obtain formate, studies in flow-cell operating in
116 a continuous mode with a higher j than that reported previously are definitely needed.
117 Alike, an assessment of the formate concentration and consumption of energy must also
118 be carried out, since achieving high product concentration with an energy consumption
119 as low as possible will be necessary for the application at commercial scale in the future.

120 In this context, here we study the CO_2 electrocatalytic reduction to obtain formate
121 working in a continuous mode using carbon-supported Bi nanoparticles (Bi/C-NPs) as
122 electrocatalytic material, operating at j of up to $300 \text{ mA}\cdot\text{cm}^{-2}$ in an innovative system with
123 a filter-press electrochemical cell to allow high efficiencies with a single pass of the

124 catholyte through the cell. The performance of Gas Diffusion Electrodes (Bi-GDEs),
125 prepared using the previous synthesized and characterized Bi/C-NPs, was assessed in a
126 continuous flow-cell electrochemical reactor, with only a single pass of the electrolyte.
127 Moreover, the influence of some important variables such as j and electrolyte flow per
128 geometric surface area (Q/A) on the performance of the process was studied.

129

130 **2. Methodology**

131 2.1 Synthesis and characterisation of Bi NPs

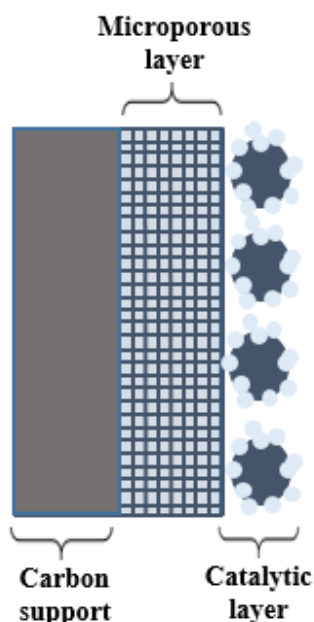
132 Carbon-supported Bi nanoparticles (Bi/C-NPs) were prepared as described in detail in
133 another contribution [67]. Very briefly, 0.316 g of BiCl₃ (99.99%, Aldrich) and 0.112 g
134 of polyvinylpyrrolidone (PVP, K30, Mw ~55.000, Aldrich) were added into 37.92 g of
135 N,N-Dimethylformamide (DMF, 99.8%, Sigma Aldrich) and sonicated until complete
136 solubilisation. Then, 0.116 g of NaBH₄ (99%, Aldrich) were added to the solution at room
137 temperature (20°C) and under continuous magnetic stirring. The solution was
138 magnetically stirred and sonicated (Selecta ultrasonic bath operating at 50/60 kHz, 360
139 power output) for at least 15 min. Subsequently, 0.836 g of carbon Vulcan XC-72R were
140 added to the mixture to obtain a Bi loading of ca. 20 wt.%. The sample is then
141 continuously sonicated during 60 min to properly dispersed the Bi nanoparticle on the
142 carbon substrate. The sample is precipitated by adding acetone, and filtered and washed
143 also with acetone, and finally dried overnight under vacuum conditions at 45 °C.

144 Transmission electron microscopy (TEM) images were obtained with a JEOL JEM-2010
145 microscope, working at 200 kV and with a JEOL JEM-1400 Plus working at 120 kV to
146 evaluate the size of the particle and dispersion of the Bi nanoparticles. The metal (Bi)
147 loading was experimentally measured by atomic absorption spectroscopy (AAS) using a

148 SpectrAA-220 FS. A known amount of the Bi/C-NPs was treated in nitric acid and then
149 filtered. The sample was then conveniently diluted using a 2 wt% HNO₃ water solution.

150 2.2 Bi-GDE fabrication and characterization

151 In the electrochemical reactor, Bi-GDE was used as working electrode. Bi/C NPs,
152 previously synthesized and characterized as explained in Section 2.1, have been used as
153 catalyst in Bi-GDE. A carbonaceous support (TGP-H-60), a microporous layer (MPL)
154 and the catalytic layer (CL) shaped the Bi-GDE configuration, as shown in Fig. 1. The
155 geometric surface area of the Bi-GDE was 10 cm².



156

157

Fig 1. Scheme of the Bi-GDE configuration.

158 A Toray carbon paper was used as TGP-H-60 (Teflonated Paper, TGP-H-60). Firstly, a
159 MPL was air-brushed over the carbonaceous support. An ink was prepared with Vulcan
160 XC-72R and PTFE (Polytetrafluoroethylene preparation, 60 wt.% dispersion in H₂O,
161 Sigma-Aldrich) in a ratio of 40/60, and then diluted in isopropanol in a final slurry of 3
162 wt.%. The ink was sonicated during 30 minutes before it was sprayed with the air-brusher.

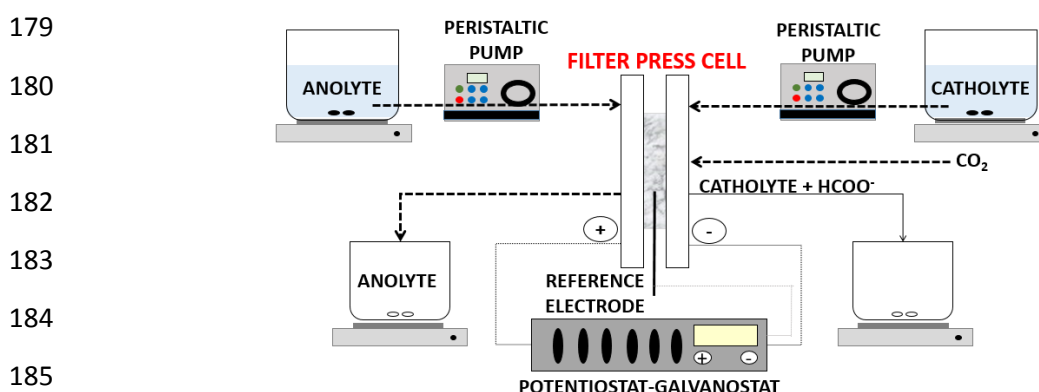
163 When the microporous layer reached a Vulcan XC-72R loading of $2 \text{ mg} \cdot \text{cm}^{-2}$, both layers
164 were sintered at $350 \text{ }^\circ\text{C}$ during 1800 seconds.

165 Subsequently, a CL was sprayed over the microporous layer by an air-brushing technique.
166 The catalytic ink consisted of Bi/C NPs in Nafion (Nafion D-521 dispersion, 5% w/w in
167 water and 1-propanol, $\geq 0,92 \text{ meq/g}$ exchange capacity) with ratio of 70/30, which were
168 then diluted in isopropanol and sonicated in the same conditions as described previously
169 for the microporous layer. The Bi/C NPs loading was $0.75 \text{ mg} \cdot \text{cm}^{-2}$.

170 Scanning electron microscopy (SEM, HITACHI S-3000 N micro-scope working at 20 kV
171 with X-ray detector Bruker Xflash 3001 for microanalysis) was employed to characterise
172 the Bi-GDEs.

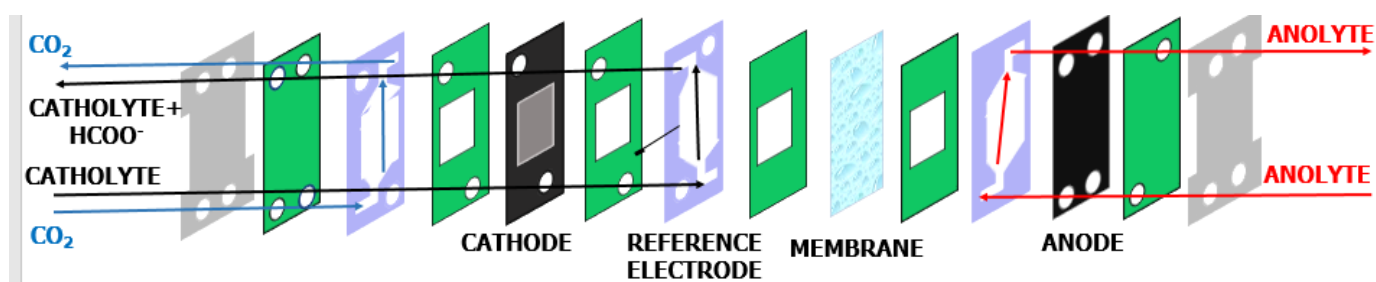
173 2.3 Filter press tests

174 The Bi-GDEs prepared and characterized were then used as working electrodes in an
175 innovative continuous system with a filter press electrochemical cell. Apart from the filter
176 press cell (Micro Flow Cell, ElectroCell A/s), the experimental set-up included peristaltic
177 pumps (Watson Marlow 320, Watson Marlow Pumps Group), tanks and a potentiostat-
178 galvanostat (Arbin Instruments, MSTAT4), as shown in Fig. 2.



186 **Fig. 2.** Experimental set up used for the tests of Bi-GDEs for the continuous CO_2
187 electrocatalytic reduction to give formate.

188 Figure 3 represents a scheme of the cell. The internal structure of the filter press cell can
 189 be seen in figure S1 of the Supporting Information to improve the understanding of this
 190 electrochemical reactor. In this configuration, both compartments are separated by a
 191 cation exchange membrane, Nafion 117, which allows cations to cross from the anodic
 192 compartment to the cathodic compartment. The electrocatalytic reduction of CO₂ takes
 193 place in the cathode. Moreover, the electrolyte used in this compartment was a solution
 194 of 0.5 M KCl + 0.45 M KHCO₃. In addition, pure carbon dioxide was fed to the cathodic
 195 compartment at a flow rate of 200 mL·min⁻¹.
 196 The anolyte used in the anodic compartment, was a 1M KOH solution with a Q/A of 0.57
 197 mL·min⁻¹·cm⁻². Moreover, a dimensionally stable anode, [DSA/O₂(Ir-MMO (mixed
 198 metal oxide) on platinum))] was used as counter electrode.



199 **Fig 3.** Filter press cell configuration used for the continuous CO₂ electrocatalytic
 200 reduction to give formate using Bi-GDEs.

201 As reference electrode, a leak-free Ag/AgCl 3.4 M KCl was also placed near the working
 202 electrode, in the cathodic compartment.

203 Experiments were performed in a continuous mode with a single pass of the catholyte and
 204 anolyte across the cell. Moreover, during 5400 seconds experiments were executed at
 205 ambient pressure (101325 Pa) and temperature (20°C). The main variables studied were
 206 Q/A and j, which was supplied by the potentiostat-galvanostat. Each 30 minutes, samples
 207 were taken by duplicate. Concentration of formate was analysed by ion chromatograph
 208 (Dionex ICS 1100 equipped with an AS9-HC column, using Na₂CO₃ as the eluent with a

209 concentration, flow-rate, conductivity and pressure of 4.5 mM, 1 mL·min⁻¹, 15 μS and
210 1800 psi, respectively).

211 A mean value of formate concentration was obtained for each experiment in order to
212 determine the FE, rate and consumption of energy (CE). The FE is described as the total
213 charge supplied by the potentiostat that is applied to obtain the desired product, formate
214 in this case [68]. The FE can be calculated by equation (1):

$$215 \quad \text{FE}(\%) = \frac{z \cdot F \cdot C_{\text{HCOO}^-}}{Q} \cdot 100 \quad (1)$$

216 where z is the number of electrons exchanged in the electrochemical process, F is the
217 Faraday constant (96485·mol⁻¹), C_{HCOO^-} is the molar flow rate of formate (mol·s⁻¹) and Q
218 is defined as the total charge supplied by potentiostat-galvanostat (A).

219 The rate of formate production expressed the total amount of formate per unit of working
220 electrode area and unit of time, defined by equation (2):

$$221 \quad \text{Rate} \left(\frac{\text{mol}}{\text{m}^2 \text{ s}} \right) = \frac{C_{\text{HCOO}^-}}{A} \quad (2)$$

222 where C_{HCOO^-} is also the molar flow of formate obtained in each experiment (mol·s⁻¹) and
223 A is the geometric surface area of the working electrode (m²).

224 The CE was expressed as the amount of energy used in the electrochemical reactor to
225 produce a certain amount of formate. (i.e. kWh per kmol). The CE can be calculated by
226 equation (3):

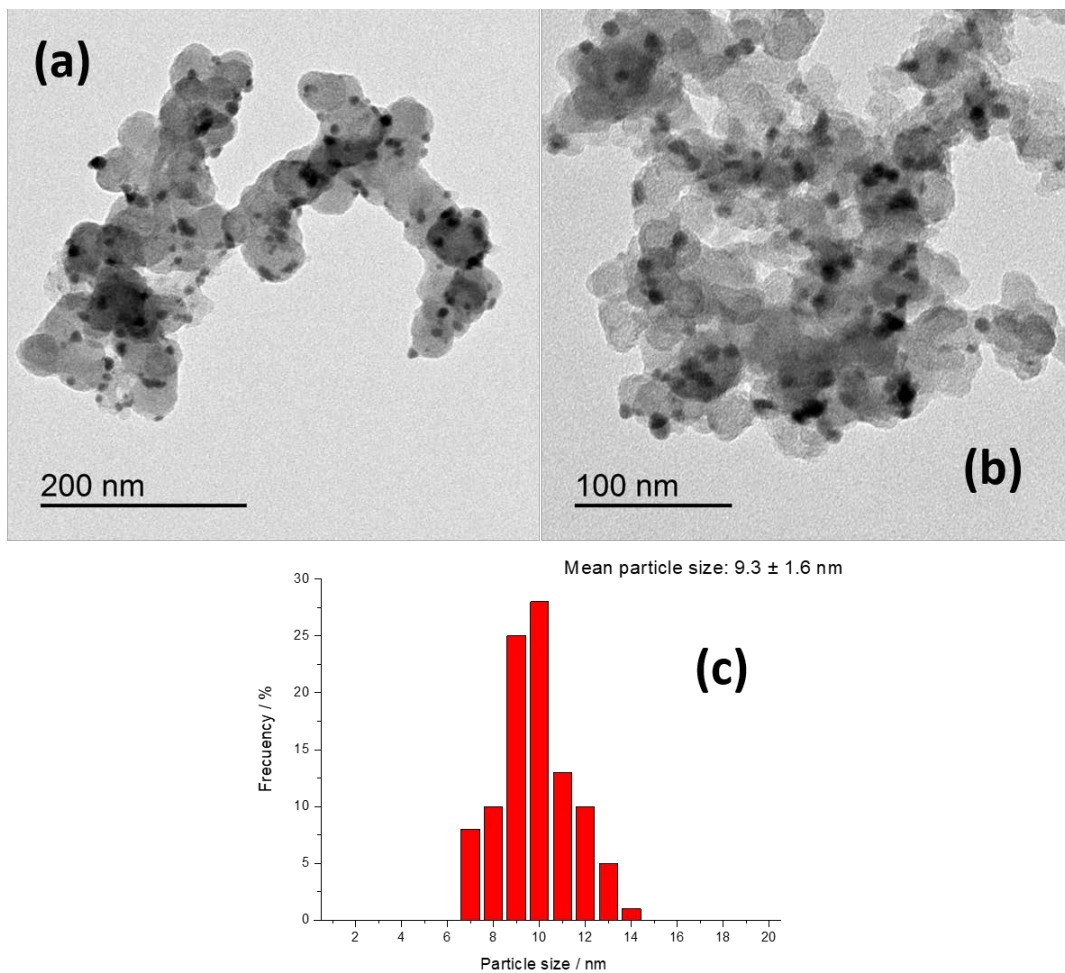
$$227 \quad \text{CE} \left(\frac{\text{kWh}}{\text{kmol}} \right) = \frac{Q \cdot V}{C_{\text{HCOO}^-}} \quad (3)$$

228 where Q and C_{HCOO^-} have the same meaning as in equation (1) and (2) and V is the
229 absolute potential in the filter-press cell (V).

230 **3. Results**

231 3.1 Bi/C NPs characterization

232 Figures 4a and 4b show some representative TEM images of the Bi/C NPs. As shown by
233 the corresponding histogram (figure 4c), the particle size is 9.3 ± 1.6 nm. As expected,
234 the Bi NPs display a quasi-spherical shape and a good distribution on the carbon substrate.
235 The metal loading was found to be about 15 ± 1 wt. %, slightly lower than the nominal
236 one.



237

238 **Fig 4.** (a-b) TEM images and (c) particle size histogram corresponding to the Bi/C NPs.

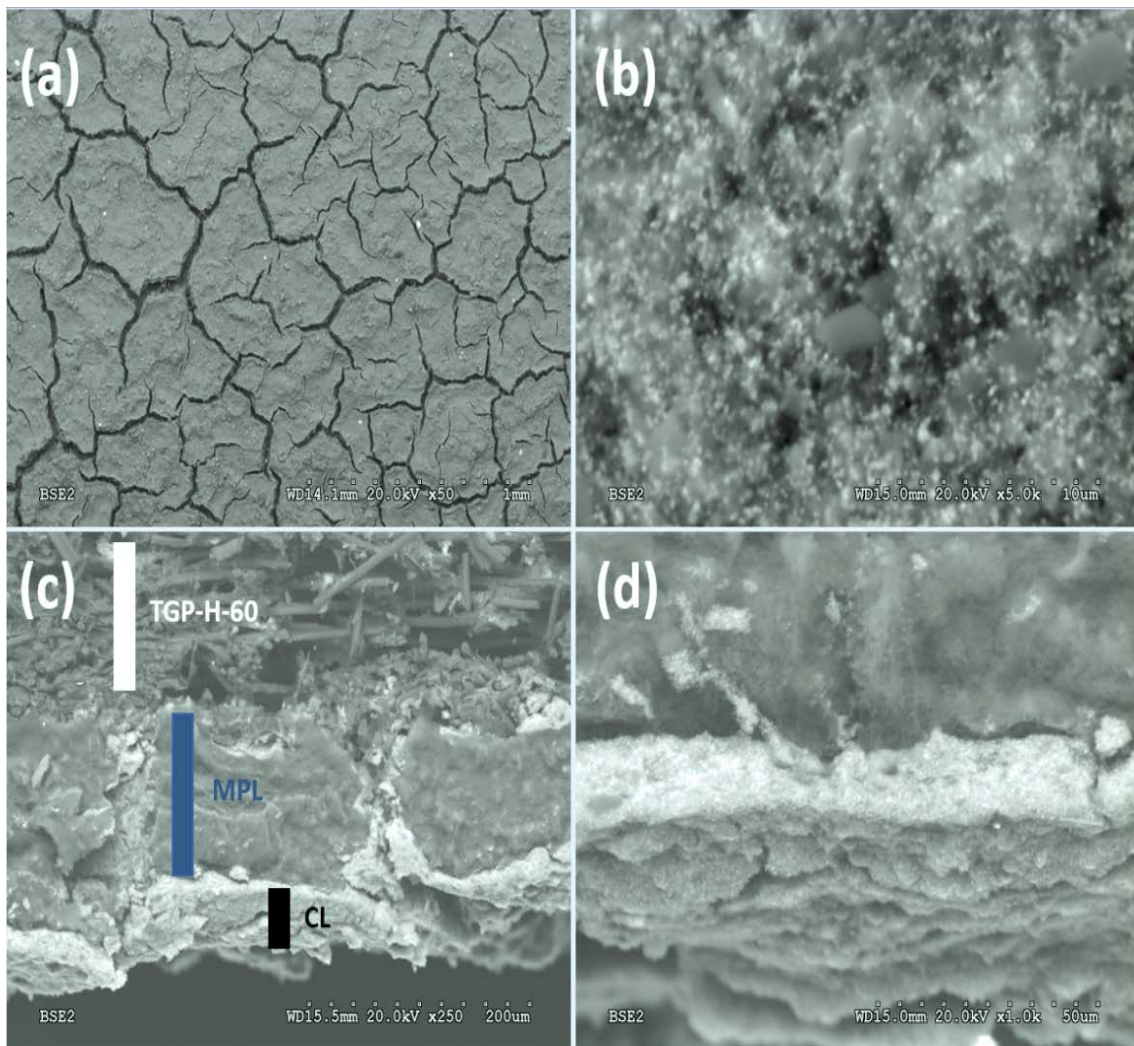
239

240

241

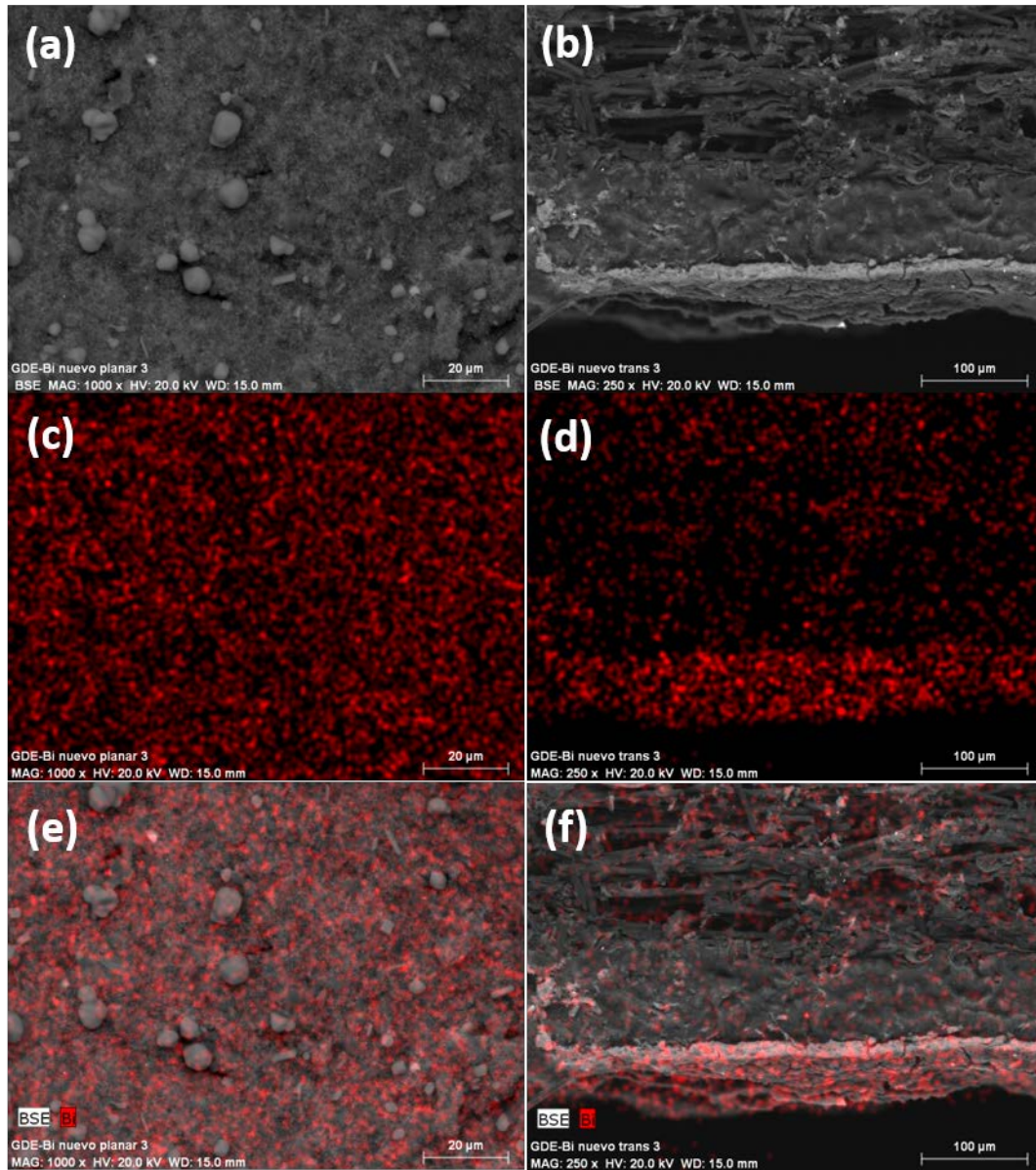
242 3.2 Bi-GDE characterization

243 The Bi GDEs were also characterized (surface and cross section) by SEM/EDX. Figure
244 5 reports some representative SEM images obtained using backscattered electrons. Figure
245 5a shows a low magnification SEM image of the surface of the Bi GDE. The deposit
246 seems uniform although some fractures are clearly visible. At much higher magnification
247 (figure 5b), it is even possible to visualize the good dispersion of the Bi nanoparticles. On
248 the other hand, from the analysis of the cross-section SEM images (figures 5b and 5c),
249 the thickness of the MPL and the CL can be analysed. The thickness of the MPL and CL
250 are estimated to be about 100-125 μm and 15-20 μm , respectively.



251 **Fig 5.** SEM images of the Bi-GDEs, (a, b) surface and (c, d) cross section.

252 To complete this analysis, figure 6 displays some SEM/EDX images of the Bi-GDEs. In
253 both cases (surface and cross section), the EDX mapping shows a homogeneous
254 distribution of the Bi nanoparticles.



255

256 **Fig 6.** SEM/EDX images of the Bi-GDEs, (a, c, d) surface and (b, d, f) cross section.

257

258

259

260 3.3 Filter press reactor tests

261 In table 1, the main results obtained in this study are summarized with the conditions
262 explained in last subsections.

263 **Table 1.** Results of Bi-GDE obtained operating in continuous reactor with only a single
264 pass of the electrolyte. Electrode catalyst loading: $0.75 \text{ mg}\cdot\text{cm}^{-2}$ of Bi carbon supported
265 nanoparticles.

266

Point	Current density, j (mA cm^{-2})	Electrolyte flow/area, Q/A ($\text{mL}\cdot\text{min}^{-1}\cdot\text{cm}^{-2}$)	Average HCOO^- concentration, ($\text{g}\cdot\text{L}^{-1}$)	Average faradaic efficiency, FE (%)	Average HCOO^- rate, r ($\text{mmol}\cdot\text{m}^{-2}\cdot\text{s}^{-1}$)	Average energy consumption, CE ($\text{kWh}\cdot\text{kmol}^{-1}$)	Standard deviation (%)	Cathode potential (V)	Absolute cell potential (V)
1	90	0.57	2.04	92.4	4.31	177	7.27	-1.3	3.1
2	150	0.57	3.06	83.1	6.46	240	9.86	-1.5	3.7
3	200	0.57	3.95	80.4	8.33	277	1.80	-1.6	4.2
4	300	0.57	5.20	70.6	10.97	410	2.63	-2.5	5.4
5	90	0.15	7.51	89.5	4.18	186	6.49	-1.3	3.1
6	200	0.15	11.70	62.7	6.5	364	3.79	-1.6	4.3
7	200	0.07	18.02	45.1	4.67	535	2.15	-1.9	4.5

267 Different filter press experiments were carried out in order to study the influence of the j
268 and the Q/A. First, tests at an Q/A of $0.57 \text{ mL}\cdot\text{min}^{-1}\cdot\text{cm}^{-2}$ and different j were carried out.
269 Working at 90 mA cm^{-2} and $0.57 \text{ mL}\cdot\text{min}^{-1}\cdot\text{cm}^{-2}$, an excellent value of FE of 92.4 % was
270 achieved, with a rate of $4.31 \text{ mmol}\cdot\text{m}^{-2}\cdot\text{s}^{-1}$ (point 1). As shown in Table 1, concentration
271 of formate increased, when j was increased from 90 to $300 \text{ mA}\cdot\text{cm}^{-2}$ (Table 1, point 4),
272 from 2.04 to $5.20 \text{ g formate}\cdot\text{L}^{-1}$, which represents an increase of 155%.

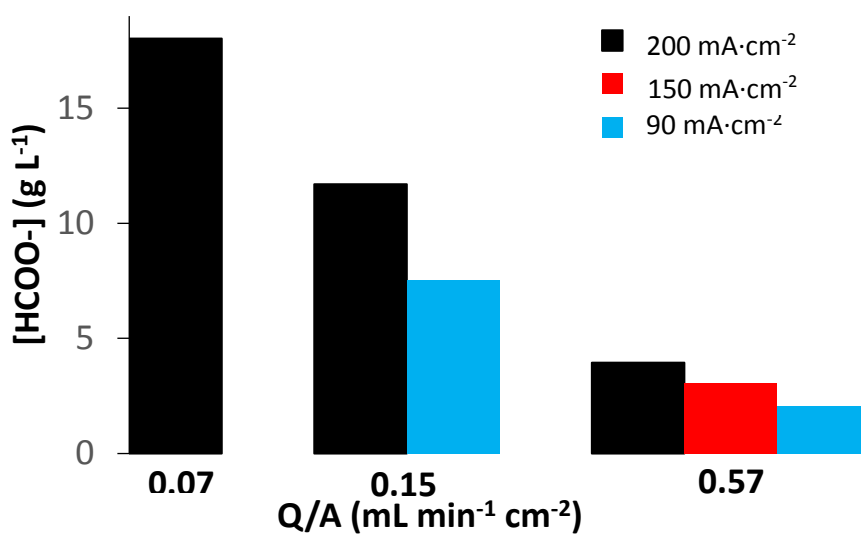
273 Although concentration of formate was increased, FE lowered approximately 20 points
274 in percentage (from 92.4 to 70.6%) when j was raised from 90 to $300 \text{ mA}\cdot\text{cm}^{-2}$. As middle
275 points, tests were carried out at 150 and $200 \text{ mA}\cdot\text{cm}^{-2}$ (point 2 – 3), giving FEs around 80
276 %.

277 Even though increasing j resulted in less FE, there was an important rise in the value of
278 formate rate obtained. If at $90 \text{ mA}\cdot\text{cm}^{-2}$ the formate rate achieved was $4.31 \text{ mmol}\cdot\text{m}^{-2}\cdot\text{s}^{-1}$

279 ¹, increasing the j to $150 \text{ mA}\cdot\text{cm}^{-2}$ was beneficial to the process, giving a rate more than
280 50% higher than the value of rate obtained working at $90 \text{ mA}\cdot\text{cm}^{-2}$. This rising in formate
281 rate was also observed when j was increased to 200 and $300 \text{ mA}\cdot\text{cm}^{-2}$, resulting in a rate
282 value of 8.33 and $10.97 \text{ mmol}\cdot\text{m}^{-2}\cdot\text{s}^{-1}$, respectively.

283 In terms of CE, the results obtained show that j and absolute potential in the
284 electrochemical reactor affect CE in a proportional way (see values in Table 1). The CE
285 per kmol of formate of $177 \text{ kWh kmol}^{-1}$ was achieved with a j of $90 \text{ mA}\cdot\text{cm}^{-2}$, which
286 corresponds to an energy efficiency towards formate of 30%. However, working with a
287 higher j of 150, 200 or $300 \text{ mA}\cdot\text{cm}^{-2}$, the CE per kmol of formate increased proportionally
288 in more than 35%, 55% and 125% with respect to the value of j of $90 \text{ mA}\cdot\text{cm}^{-2}$.

289 Operating in a continuous mode with a j as high as possible, and keeping high efficiencies,
290 have been suggested as requirements for the industrial implementation of this type of CO_2
291 electroconversion process. Moreover, concentration of formate must also be as high as
292 possible, since studies have shown that the energy needed to concentrate the formate
293 solution obtained from the CO_2 electrochemical conversion process until levels of
294 commercial interest will definitely play an important function in the feasibility of this
295 electrochemical process at industrial scale [69,70]. Consequently, the influence of Q/A
296 was further analysed in order to obtain a formate product as concentrated as possible.
297 Graphs have been included in Fig. 7 and 8 to allow for a clearer visualization of the results
298 of formate concentration and FE achieved.



299

300

Fig. 7. Concentration of formate as a function of the j and Q/A .

301

As illustrated in Fig. 7, concentration of formate obtained raised approximately 4 times

302

(from 2.04 to 7.51 g formate·L⁻¹) when the Q/A decreased from 0.57 to 0.15 mL·min⁻¹

303

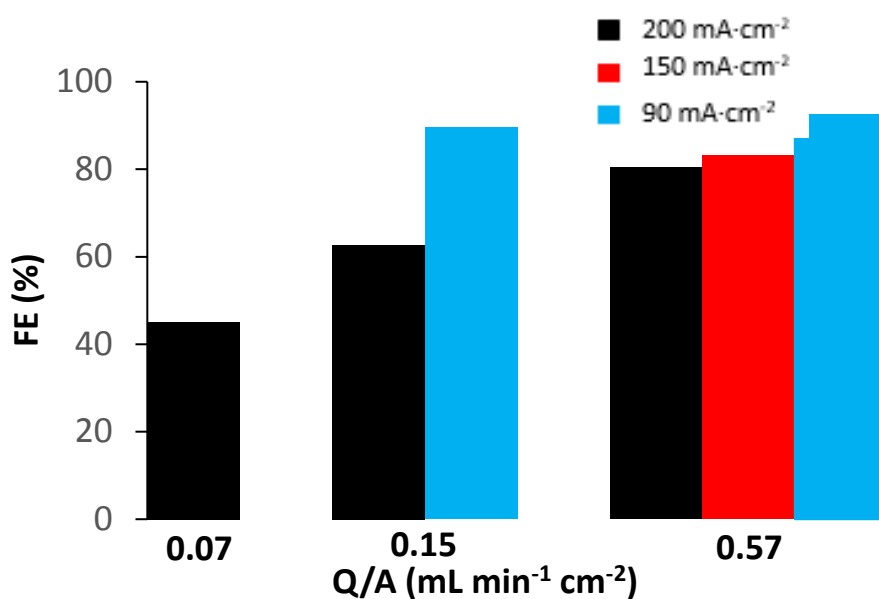
·cm⁻², working at 90 mA·cm⁻². Even though reducing the Q/A provides higher

304

concentration of formate, FE and formate rate keep similar values, around 90% and 4.25

305

mmol·m⁻²·s⁻¹, respectively.



306

307

Fig. 8. FE as a function of the j and Q/A .

308 The same analysis was carried out working with a j of $200 \text{ mA}\cdot\text{cm}^{-2}$. The formate
 309 concentration increased from 3.95 to $11.70 \text{ g formate}\cdot\text{L}^{-1}$, when the electrolyte Q/A was
 310 reduced from 0.57 to $0.15 \text{ mL}\cdot\text{min}^{-1}\cdot\text{cm}^{-2}$. By decreasing Q/A, a decline of FE (as shown
 311 in Fig. 8) and formate rate values happened, from 80% and $8.33 \text{ mmol}\cdot\text{m}^{-2}\cdot\text{s}^{-1}$ to 63% and
 312 $6.50 \text{ mmol}\cdot\text{m}^{-2}\cdot\text{s}^{-1}$ respectively. A maximum concentration of $18.02 \text{ g formate}\cdot\text{L}^{-1}$ was
 313 achieved with an additional drop of Q/A to $0.07 \text{ mL}\cdot\text{min}^{-1}\cdot\text{cm}^{-2}$. Although working with
 314 this value of Q/A provides the highest formate concentration, FE and rate of production
 315 had an important drop of 50% with respect to the scenario of working with an Q/A of
 316 $0.57 \text{ mL}\cdot\text{min}^{-1}\cdot\text{cm}^{-2}$, from 80% and $8.33 \text{ mmol}\cdot\text{m}^{-2}\cdot\text{s}^{-1}$ to 45% and $4.67 \text{ mmol}\cdot\text{m}^{-2}\cdot\text{s}^{-1}$.

317 Finally, Table 2 summarizes the results of this study and the best results reported in
 318 literature for the electrocatalytic reduction of CO_2 to give formate or formic acid,
 319 including the product concentration or the FE obtained and the j employed in the
 320 electrochemical process. It is important to remark that different operating conditions and
 321 cell configurations are applied in each study.

322 Table 2. Summary of best results reported in literature for the electrocatalytic reduction
 323 of CO_2 to obtain formate or formic acid: concentration, FE and rate

324

Electrocatalyst	Electrode	Average HCOO^- concentration, ($\text{g}\cdot\text{L}^{-1}$)	Average faradaic efficiency, FE (%)	Average HCOO^- rate, r ($\text{mmol}\cdot\text{m}^{-2}\cdot\text{s}^{-1}$)	Current density, j ($\text{mA}\cdot\text{cm}^{-2}$)	Absolute cell potential (V)	Reference
Bi/C - NPs	GDE	7.51	89.5	4.18	90	3.1	This work
Sn/C NPs	GDE	5.05	60.2	2.81	90	3.0	[36]
Sn	GDE	205	32	4.63	140	3.3	[38] ^a
Sn	Metal plate	17.2	55		50		[40] ^b
Sn	Metal plate	20	65		100	4	[71] ^b
Sn	CCME	19.2	49.4	1.15	45	2.2	[72] ^c
Sn	CCME	41.5	93.3		51.7	2.2	[41] ^c

325 ^aThe electrochemical reactor utilises a Dioxide Materials Sustainion™ anion exchange membrane

326 ^bA high pressure electrochemical reactor is used.

327 ^cElectrocatalytic reduction of CO₂ to give formate is done operating in a gaseous phase.

328 As can be noted in Table 2, the best results reported previously in the literature have been
329 obtained using Sn as electrocatalyst. This catalyst has been greatly investigated for this
330 application, and these research efforts have led to reactor designs and operational
331 conditions optimized for Sn-based catalysts. The results achieved with the Bi/C NPs
332 studied in this work, although still lower than the best results with Sn, are promising,
333 particularly considering that the reactor design and the operational conditions are yet to
334 be optimized for Bi-based electrocatalysts.

335 Moreover, as can be noted looking at Table S1, the results reported in this paper are
336 especially noteworthy when compared with previous studies using Bi, which had not
337 worked in a continuous mode with high values of current density supplied.

338 Recent studies on electrochemical valorisation of CO₂ to formate using Bi as catalyst have
339 been carried out in a discontinuous mode in a two-compartment electrochemical reactor.

340 It is important to remark that the results of this study have been obtained in an innovative
341 continuous system with a filter press cell working with j up to $300 \text{ mA}\cdot\text{cm}^{-2}$, greater than
342 j reported in literature. The results obtained in this work confirm that the Bi-GDEs allow
343 working in a continuous electrochemical cell with higher j values compared with recent
344 contributions, compulsory for the technical viability of CO₂ electrocatalytic reduction,
345 keeping reasonable values of formate concentration, FE, rate and CE per kmol of product.

346 Moreover, on the one hand concentration of formate can be even increased at the expense
347 of decreasing FE and rate or increasing CE per kmol of formate, as shown in Fig. 7. On
348 the other hand, as illustrated in Table 2, the performance of the electrochemical process
349 could be enhanced optimizing the reactor design and the operating conditions.

350

351 **4. Conclusions**

352 This work presents novel results on CO₂ electrovalorisation towards formate working in
353 a continuous mode in a filter press cell using Bi-GDEs. Bi-GDEs were fabricated using
354 Bi/C-NPs, which were synthesized and characterized. Bi-GDEs were able to work at a j
355 up to 300 mA·cm⁻², obtaining 5.2 g formate·L⁻¹ with FE of 70 % and rate of 11 mmol·m⁻²·
356 s⁻¹. Decreasing j to 90 mA·cm⁻², the concentration obtained was 7.5 g formate·L⁻¹ with
357 an increase of FE up to 90% and CE of only 186 kWh kmol⁻¹. Moreover, the highest
358 concentration of formate obtained is 18 g L⁻¹, but with an important decrease in FE
359 compared with other points. It is important to emphasise that these results were obtained
360 working at higher j than previous studies in the literature, and they also were obtained
361 working in a continuous mode with only a single pass of the catholyte across the filter
362 press cell. These conditions are compulsory to remark the feasibility of the process using
363 Bi/C-NPs in Bi-GDEs.

364 Finally, results from this work are promising but more research is needed. A future step
365 to further improve this process of electrocatalytic conversion of CO₂ to formate would be
366 to work in gas phase using the electrode configuration so called “Catalyst Coated
367 Membrane Electrode”, in which the promising Bi/C-NPs, described in this paper could
368 be deposited directly over membrane. With this configuration, formate concentration
369 should be increased, while at the same time, CE per kmol of formate shall be lower.

370

371 **Acknowledgments**

372 The authors of this work would like to show their gratitude to the financial support from
373 the MINECO, through the projects CTQ2016-76231-C2-1-R and CTQ2016-76231-C2-
374 2-R (AEI/FEDER, UE). Jose Solla-Gullón also acknowledges the financial support from
375 VITC of the University of Alicante (UTALENTO16-02).

376 **References**

377

- 378 [1] US Department of Commerce NESRL. ESRL Global Monitoring Division - Global
379 Greenhouse Gas Reference Network n.d. (accessed February 20, 2019)
- 380 [2] Zhang W, Hu Y, Ma L, Zhu G, Wang Y, Xue X, et al. *Adv Sci* 2018;5:1700275.
- 381 [3] Alvarez-Guerra M, Albo J, Alvarez-Guerra E, Irabien A. *Energy Environ Sci*
382 2015;8:2574–99.
- 383 [4] Qiao J, Liu Y, Zhan J. *Electrochemical Reduction of Carbon Dioxide.*
384 *Fundamentals and Technologies*, CRC Press, Boca Raton, FL, 2016.
- 385 [5] Bevilacqua M, Filippi J, Miller HA, Vizza F. *Energy Technol* 2015;3:197–210. 6.
- 386 [6] Albo J, Alvarez-Guerra M, Castaño P, Irabien A. *Green Chem* 2015;17:2304–24.
- 387 [7] Merino-Garcia I, Alvarez-Guerra E, Albo J, Irabien A. *Chem Eng J* 2016;305:104–
388 20.
- 389 [8] Kumar B, Brian JP, Atla V, Kumari S, Bertram KA, White RT, et al. *Catal Today*
390 2016;270:19–30.
- 391 [9] Martín AJ, Larrazábal GO, Pérez-Ramírez J. *Green Chem* 2015;17:5114–30.
- 392 [10] Irabien A, Alvarez-Guerra M, Albo J, Dominguez-Ramos A. *Electrochemical*
393 *Conversion of CO₂ to Value-Added Products.* In: Martínez-Huitle CA, Rodrigo
394 MA, Scialdone, O, editors. *Electrochem. Water Wastewater Treat.*, Elsevier; 2018,
395 p. 29–59.
- 396 [11] Hori, Y. *Reduction Using Electrochemical Approach*, In: Sugiyama M, Fujii, K,
397 Nakamura, S, editors. *Solar to Chemical Energy Conversion: Theory and*
398 *Application*, Cham, 2016, p. 191-211.

- 399 [12] Lu Q, Jiao F. *Nano Energy* 2016;29:439–56.
- 400 [13] Jones JP, Prakash GKS, Olah GA. *Isr J Chem* 2014;54:1451–66.
- 401 [14] Wang Q, Dong H, Yu H, Yu H, Liu M. *RSC Adv* 2015;5:10346–51.
- 402 [15] Grace AN, Choi SY, Vinoba M, Bhagiyalakshmi M, Chu DH, Yoon Y, et al. *Appl*
403 *Energy* 2014;120:85–94.
- 404 [16] Kraus GA. *Commercializing Biobased Products: Opportunities, Challenges,*
405 *Benefits, and Risks.* 2015.
- 406 [17] Zhang T, Zhong H, Qiu Y, Li X, Zhang H. *J Mater Chem A* 2016;4:16670–6.
- 407 [18] Wang C, Cao M, Jiang X, Wang M, Shen Y. *Electrochim Acta* 2018;271:544–50.
- 408 [19] Merino-Garcia I, Albo J, Irabien A. *Energy Technol* 2017;5:922–8.
- 409 [20] Merino-Garcia I, Albo J, Irabien A. *Nanotechnology* 2018;014001.
- 410 [21] Yuan J, Yang MP, Hu QL, Li SM, Wang H, Lu JX. *J CO₂ Util* 2018;24:334–40.
- 411 [22] Albo J, Sáez A, Solla-Gullón J, Montiel V, Irabien A. *Appl Catal B Environ*
412 *2015;176–177:709–17.*
- 413 [23] Taheri A, Berben LA. *Chem Commun* 2016;52:1768–77.
- 414 [24] Du D, Lan R, Humphreys J, Tao S.. *J Appl Electrochem* 2017;47:661–78.
- 415 [25] Preuster P, Albert J. *Energy Technol* 2018;6:501–9.
- 416 [26] Müller K, Brooks K, Autrey T. *Energy and Fuels* 2017;31:12603–11.
- 417 [27] An L, Chen R. *J Power Sources* 2016;320:127–39.
- 418 [28] Wang LQ, Bellini M, Filippi J, Folliero M, Lavacchi A, Innocenti M, et al. *Appl*
419 *Energy* 2016;175:479–87.

- 420 [29] Alvarez-Guerra M, Quintanilla S, Irabien A. *Chem Eng J* 2012;207-208:278-84.
- 421 [30] Mou K, Chen Z, Yao S, Liu L. *Electrochim Acta* 2018;289:65–71.
- 422 [31] Gao S, Lin Y, Jiao X, Sun Y, Luo Q, Zhang W, et al. *Nature* 2016;529:68–71.
- 423 [32] Bai X, Chen W, Zhao C, Li S, Song Y, Ge R, et al. *Angew Chemie - Int Ed*
424 2017;56:12219–23.
- 425 [33] Alvarez-Guerra M, Del Castillo A, Irabien A. *Chem Eng Res Des* 2014;92:692-701.
- 426 [34] Del Castillo A, Alvarez-Guerra M, Irabien A. *AIChE J* 2014;60(10):3557-64.
- 427 [35] Del Castillo A, Alvarez-Guerra M, Solla-Gullón J, Sáez A, Montiel V, Irabien A.
428 *Appl Energy* 2015;157:165-73
- 429 [36] Castillo A Del, Alvarez-Guerra M, Solla-Gullón J, Sáez A, Montiel V, Irabien A.
430 *J CO₂ Util* 2017;18:222–8.
- 431 [37] Kopljar D, Inan A, Vindayer P, Wagner N, Klemm E. *J Appl Electrochem*
432 2014;44:1107-16.
- 433 [38] Yang H, Kaczur JJ, Sajjad SD, Masel RI. *ECS Trans* 2017;77:1425–31.
- 434 [39] Fu Y, Li Y, Zhang X, Liu Y, Qiao J, Zhang J, et al. *Appl Energy* 2016;175:536-
435 44.
- 436 [40] Proietto F, Schiavo B, Galia A, Scialdone O. *Electrochimic Acta* 2018;277:30-40.
- 437 [41] Lee W, Kim Y, Youn M, Jeong S, Park K. *Angew Chemie - Int Ed*
438 2018;57:6883:87.
- 439 [42] Zhang H, Ma Y, Quan F, Huang J, Jia F, Zhang L. *Electrochem Commun*
440 2014;46:63–6.

- 441 [43] Zhong H, Qiu Y, Zhang T, Li X, Zhang H, Chen X. *J Mater Chem A*
442 2016;4:13746–53.
- 443 [44] Koh JH, Won DH, Eom T, Kim NK, Jung KD, Kim H, et al. *ACS Catal*
444 2017;7:5071–7.
- 445 [45] Lv W, Zhou J, Bei J, Zhang R, Wang L, Xu Q, et al. *Appl Surf Sci* 2017;393:191–
446 6.
- 447 [46] Bertin E, Garbarino S, Roy C, Kazemi S, Guay D. *J CO₂ Util* 2017;19:276–83.
- 448 [47] Kim S, Dong WJ, Gim S, Sohn W, Park JY, Yoo CJ, et al. *S. Nano Energy*
449 2017;39:44–52.
- 450 [48] Bei J, Zhang R, Chen Z, Lv W, Wang W. *Int J Electrochem Sci* 2017;12:2365–75.
- 451 [49] Miao C-C, Yuan G-Q. *ChemElectroChem* 2018;5:3741-7.
- 452 [50] García de Arquer FP, Bushuyev OS, De Luna P, Dinh CT, Seifitokaldani A,
453 Saidaminov MI, et al. *Adv Mater* 2018;30:6–11.
- 454 [51] Qiu Y, Du J, Dai C, Dong W, Tao C. *J Electrochem Soc* 2018;165:H594–600.
- 455 [52] Lv W, Bei J, Zhang R, Wang W, Kong F, Wang L, et al. *ACS Omega* 2017;2:2561–
456 7.
- 457 [53] Han N, Wang Y, Yang H, Deng J, Wu J, Li Y, et al. *Nat Commun* 2018;9:1–8.
- 458 [54] Su P, Xu W, Qiu Y, Zhang T, Li X, Zhang H. *ChemSusChem* 2018;11:848–53.
- 459 [55] Lee CW, Hong JS, Yang KD, Jin K, Lee JH, Ahn HY, et al. *ACS Catal*
460 2018;8:931–7.
- 461 [56] Zhang Z, Chi M, Veith GM, Zhang P, Lutterman DA, Rosenthal J, et al. *ACS Catal*
462 2016;6:6255–64.

- 463 [57] Atifi A, Boyce DW, Dimeglio JL, Rosenthal J. ACS Catal 2018;8:2857–63.
- 464 [58] Zu MY, Zhang L, Wang C, Zheng LR, Yang HG. J Mater Chem A 2018;6:16804–
465 9.
- 466 [59] Zhang X, Hou X, Zhang Q, Cai Y, Liu Y, Qiao J. J Catal 2018;365:63–70.
- 467 [60] Qiu Y, Du J, Dong W, Dai C, Tao C. J CO2 Util 2017;20:328–35.
- 468 [61] Zhang X, Lei T, Liu Y, Qiao J. Appl Catal B Environ 2017;218:46–50.
- 469 [62] Zhang Y, Li F, Zhang X, Williams T, Easton CD, Bond AM, et al.. J Mater Chem
470 A 2018;6:4714–20.
- 471 [63] Shao L, Lv W, Zhang R, Kong F, Cheng L, Wang W. Int J Electrochem Sci
472 2019;14:114–25.
- 473 [64] Li L, Qifei X, Chen W, Huang S, Qifei X, Chen W, et al. Electrochim Acta
474 2019;298:580-586.
- 475 [65] Dai C, Qiu Y, He Y, Zhang Q, Liu R, Du J, et al. New J. Chemistry 2019;
476 43(8):3493-98.
- 477 [66] Zhang X, Sun X, Guo S, Bond A, Zhang J. Energy Environ. Sci. 2019; 13(4) 1334-
478 40.
- 479 [67] Ávila-Bolivar B, García-Cruz, L, Montiel V, Solla-Gullón J. Molecules, Under
480 Review.
- 481 [68] Zhu DD, Liu JL, Qiao SZ. Adv Mater 2016;28:3423-52.
- 482 [69] Dominguez-Ramos A, Singh B, Zhang X, Hertwich EG, Irabien A. J Clean Prod
483 2015;104:148–55.
- 484 [70] Rumayor M, Dominguez-Ramos A, Irabien A. F. Appl Sci 2018;8:914.

- 485 [71] Ramdin M, Morrison A, de Groen M, Van Haperen R, De Kler R, Van den Broeke
486 L, et al. Ind Eng Chem Res 2019;58:1834-57.
- 487 [72] Díaz-Sainz G, Alvarez-Guerra M, Solla-Gullon J, García-Cruz, L, Montiel V,
488 Irabien A Catal Today, Article in Press